Int. J. Electrochem. Sci., 12 **(2017)** 258 – 267, doi: 10.20964/2017.01.35

International Journal of ELECTROCHEMICAL SCIENCE
www.electrochemsci.org

Determination of Folic Acid Using Graphene/Molybdenum Disulfide Nanosheets/Gold Nanoparticles Ternary Composite

Veerappan Mani[1,2], *Mani Govindasamy*[1], *Shen-Ming Chen*[1,*], *Boopathi Subramani*[3], *Anandaraj Sathiyan*[4], *Johnson Princy Merlin*[4]

[1] Department of Chemical Engineering and Biotechnology, National Taipei University of Technology, Taipei, Taiwan 106 (ROC)
[2] Graduate Institute of Biomedical and Biochemical Engineering, National Taipei University of Technology, Taipei, Taiwan (ROC)
[3] Research Center for Applied Sciences, Academia Sinica, Nangang, Taipei 11529, Taiwan (ROC)
[4] Department of Chemistry, Bishop Heber College (Autonomous), Tiruchirappalli-620 017, Tamil Nadu, India
[*]E-mail: smchen78@ms15.hinet.net

Received: 6 October 2016 / *Accepted:* 12 November 2016 / *Published:* 12 December 2016

Currently, graphene nanosheets (GNS) and molybdenum disulfide (MoS_2) are two most popular 2D layered materials in electrochemical applications due to their excellent physico-chemical properties. Herein, we have developed a facile method to prepare a ternary nanocomposite composed of graphene, ($MoS_2$and gold nanoparticles (AuNPs) and described its electrochemical sensing applicability in the determination of folic acid (FA). The morphological, elemental, impedance and electrochemical attributes of the GNS–MoS_2–AuNPs ternary nanocomposite are studied in detail. Next, GNS–MoS_2–AuNPs is deposited on screen printed electrode (SPCE) and applied for the electrochemical sensing of folic acid. Interestingly, the composite has excellent electrocatalytic ability to folic acid due to good synergic effect between GNS, MoS_2 and AuNPs. The developed sensor detects FA in wide linear range of 50 nM–1150 µM and displays low detection limit of 38.5 nM. The sensor performance of the GNS–MoS_2–AuNPs is either superior or comparable to the previously reported electrodes. Moreover, the electrode has good repeatability, reproducibility and stability. The practical applicability of the electrode is demonstrated in human urine samples and the results have shown good recovery.

Keywords: Two dimensional layered materials; metal dichalcogenides; vitamins; nanotechnology; physical chemistry; catalysis; Analytical chemistry; Food science; carbon nanotubes

1. INTRODUCTION

For past years, graphene nanosheets (GNS), a planar two dimensional (2D) allotrope of carbon is revolutionizing the entire research community due to its peculiar physicochemical properties [1-4].

More recently, 2D layered transition metal dichalcogenides (TMDs) such as molybdenum disulfide (MoS_2) layered sheets are receiving considerable interest and their applications in catalysis is critically acclaimed [5-8]. However, MoS_2 has poor intrinsic conductivity and the sheets tend to aggregation [9-12]. Functionalization of MoS_2 with carbonaceous nanomaterials such as GNS is one of the efficient approaches in order to solve these problems, because GNS is excellent templating materials to prepare hybrid nanostructures [13-16]. More recently, Geim et al., mentioned the importance of Van der Waals heterostructures derived from GNS and MoS_2 in various applications [17]. Recent review paper summarized the various synthetical methods developed for GNS/MoS_2 hybrids and its applications in diverse areas [18]. MoS_2–GNS composites based electrochemical sensing methods are developed for the determination of human parathyroid hormone [19], NO_2 [20], acetaminophen [21], dopamine and uric acid [22], thrombin [23], oxygen reduction reaction [24] and hydrogen peroxide [25]. Studies indicated that the electrochemical sensing performance of the MoS_2 sheets can be significantly improved by the incorporation of metal nanoparticles [23, 26-28]. Herein, we have prepared gold nanoparticles (AuNPs) decorated GNS-MoS_2 composite via hydrothermal method and demonstrated its electrochemical sensing application to folic acid. First, graphene oxide (GO) was prepared and used as templates for the preparation of graphene/MoS_2. Here, the negatively charged surfaces of graphene oxide (GO) are electrostatically interacts with positively charged precursor of molybdenum [23, 29]. The following hydrothermal reaction led to the formation of MoS_2 flowers and simultaneous reduction of GO into GNS. The resulting nanostructure possesses good electrochemical attributes and excellent electrocatalytic ability to folic acid.

Folic acid (FA) (is a B-group vitamin which has a major role in biological functions of cell metabolism like DNA replication, repair and methylation, synthesis of nucleotides, vitamins, amino acids etc [30-32]. Its deficiency in our body will leads to several disorders including increased risk of colorectal cancer, neural tube defects, hypomethylation and it potentially induces proto-oncogene expression leading to cancer [33-35]. FA is available as supplements and it is to determine the amount of FA present in food and pharmaceutical. Several chemically modified electrodes are reported for the electrochemical determination of FA [30, 36-38]. In the present work, we have developed GNS–MoS_2–AuNPs ternary composite as suitable modifier on the screen printed carbon electrode for the sensitive and low-cost determination of FA.

2. EXPERIMENTAL

2.1 Chemicals and Apparatus

Graphite (powder, <20 μm), sodium molybdate dihydrate, $KAuCl_4 \cdot 3H_2O$ and all other reagents were acquired from Sigma-Aldrich. All other reagents used in this work were of analytical grade and used without additional purification. 0.1 M phosphate buffer (sodium dihydrogen phosphate and disodium hydrogen phosphate), pH 7 is employed as supporting electrolyte in electrochemical experiments.

Electrochemical studies were carried out in a three electrode cell using modified screen printed carbon electrode (SPCE) as a working electrode, saturated Ag|AgCl as a reference electrode and Pt

wire as a counter electrode. The SPCEs were purchased from Zensor R&D Co., Ltd., Taipei, Taiwan. The electrochemical measurements were performed by CHI 1205a electrochemical work station (CH Instruments, Inc., U.S.A). Prior to each electrochemical experiment, the supporting electrolytes were deoxygenated with N_2 for 10 min unless otherwise specified. Scanning electron microscopy (SEM) images were acquired using Hitachi S-3000 H scanning electron microscope Energy-dispersive X-ray spectral analysis (EDX) were acquired using Horiba Emax x-act (sensor + 24 V=16 W). The electrochemical impedance spectroscopy analyses (EIS) were performed using EIM6ex Zahner (Kronach, Germany).

2.2 Preparation of GNS/MoS_2 hybrid

Graphite oxide was prepared from graphite by following our previously published procedures and it was exfoliated to aqueous solution of graphene oxide (GO) (1 mg mL^{-1}) through ultrasonication for 1 h [39, 40]. Then, 100 mg $Na_2MoO_4.2H_2O$ and 170 mg thiourea were added and the whole solution was stirred using magnetic stirrer for 20 min [16, 41]. Afterwards, the solution was transferred into a Teflon-lined autoclave and heated to 200°C and maintained this temperature for one day. The black sediment was centrifuged, washed with copious amounts of water and ethanol successively and dried.

2.2 GNS–MoS_2–AuNPs ternary composite film modified electrode

The GNS–MoS_2 hybrid (0.5 mg mL^{-1}) was redispersed in water/ethanol mixture (40/60%) via ultrasonic agitation for 20 min. About 5 μL dispersion of GNS–MoS_2 was drop-casted on the SPCE surface and dried. Then, the GNS–MoS_2 film modified SPCE was transferred to an electrochemical cell containing 0.1 M $NaNO_3$ aqueous solution and 0.5 mM $KAuCl_4$. AuNPs were deposited through cyclic voltammetric cycling of 6 cycles. The potential range was from 0 V to + 0.9 V. The applied scan rate was 0.05 V s^{-1} [42]. Finally, the modified electrode was smoothly washed with water and dried.

3. RESULTS AND DISCUSSIONS

3.1 Characterization of GNS–MoS_2–AuNPs ternary composite

The SEM image of GNS–MoS_2 hybrid portrays densely grown sheet like morphology consists of hybrid layers of GNS and MoS_2 sheets (Figure 1A) which is consistent with previous reports [14, 43] . The SEM image of GNS–MoS_2–AuNPs composite displays the uniformly decorated AuNPs on the GNS–MoS2 hybrid surface [44]. The particle sizes ranges in 10–50 nm (Figure 1B). The EDX spectrum of GNS–MoS_2 hybrid reveals the presence of C, Mo, and S as the main components and residual quantity of O (Figure 2A). The weight percentages of C, O, Mo and S atoms are 49.89, 9.35, 18.98 and 22.77. The EDX spectrum of GNS/MoS_2/AuNPs reveals the presence of C, Mo, S and Au as

the main components and residual quantity of O (Figure 2B). The weight percentages of C, O, Mo, S and Au atoms are 42.33, 6.97, 13.18, 18.07 and 19.45.

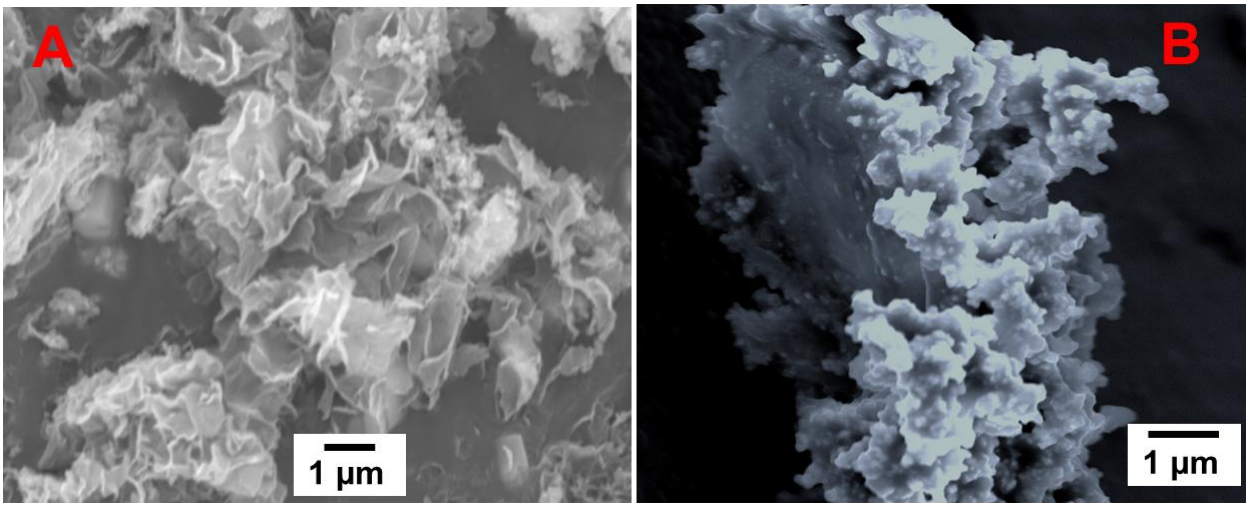

Figure 1. SEM images of GNS–MoS_2 (A) and GNS–MoS_2–AuNPs (B)

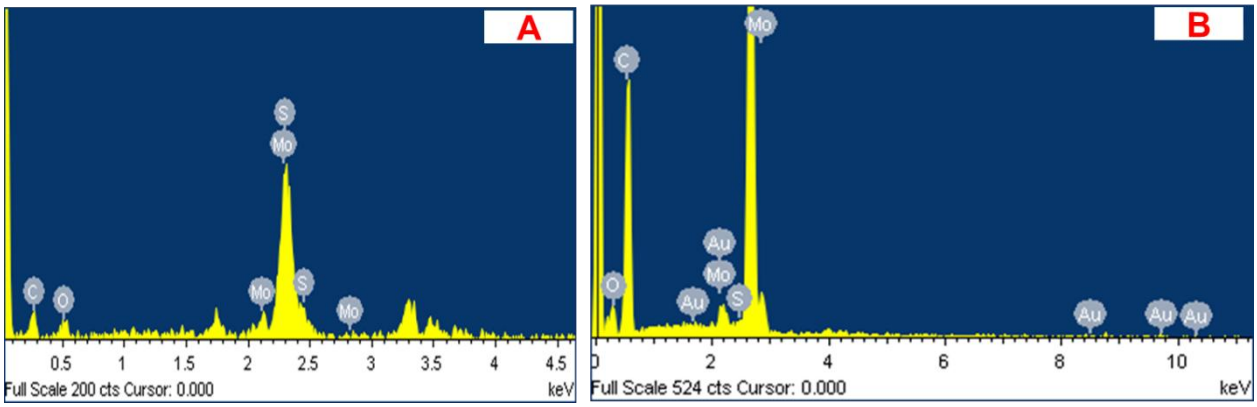

Figure 2. EDX spectra of GNS–MoS_2 (A) and GNS–MoS_2–AuNPs composite (B)

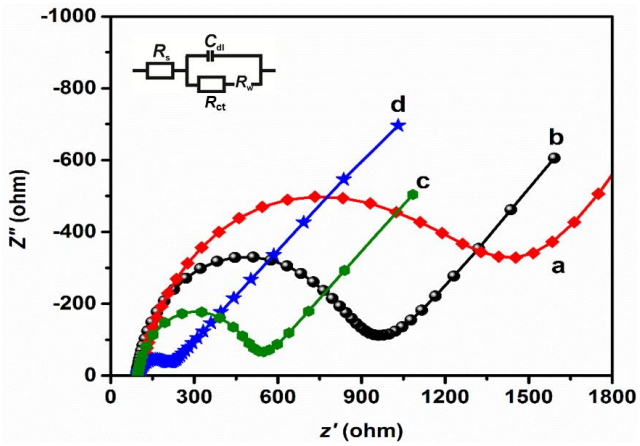

Figure 3. EIS curves of unmodified SPCE (a) MoS_2/SPCE (b), GNS–MoS_2/SPCE (c) and GNS–MoS_2–AuNPs/SPCE (d) in 0.1 M KCl containing 5 mM $Fe(CN)_6^{3-/4-}$. Amplitude: 5 mV, Frequency: 0.1 Hz to 100 kHz.

EIS analysis has been carried out to study the electrical and interfacial properties of the fabricated films modified electrodes [40, 45]. Figure 3 displays the EIS curves obtained at SPCE (a) MoS_2/SPCE (b), GNS–MoS_2/SPCE (c) and GNS–MoS_2–AuNPs/SPCE (d) in 0.1 M KCl containing 5 mM $Fe(CN)_6^{3-/4-}$. Randles equivalent circuit model was adopted to fit the experimental data wherein, R_s, R_{ct}, C_{dl} and Z_w are stands for electrolyte resistance, charge transfer resistance, double layer capacitance and Warburg impedance (inset to Figure 3). The results were exemplified as Nyquist plots. The observed semicircles portions of the EIS curves indicates the parallel combination of R_{ct} and C_{dl} at electrode surface resulting from electrode impedance and the linear portions of the curves represents diffusion limited process. The charge transfer resistance (R_{ct}) values obtained at unmodified SPCE, MoS_2/SPCE, GNS–MoS_2/SPCE and GNS–MoS_2–AuNPs/SPCE are 1411.25 Ω, 901.25 Ω, 479.73 Ω and 97.42 Ω, respectively. The R_{ct} values are in the following order; unmodified SPCE > MoS_2/SPCE > GNS–MoS_2/SPCE > GNS–MoS_2–AuNPs/SPCE, respectively. Obviously, the R_{ct} value obtained at GNS–MoS_2–AuNPs/SPCE is the lowest compared with control electrodes indicating lowest resistance at this electrode interface. Thus, the EIS results revealed that the GNS–MoS_2–AuNPs composite interface has high electrical conductivity.

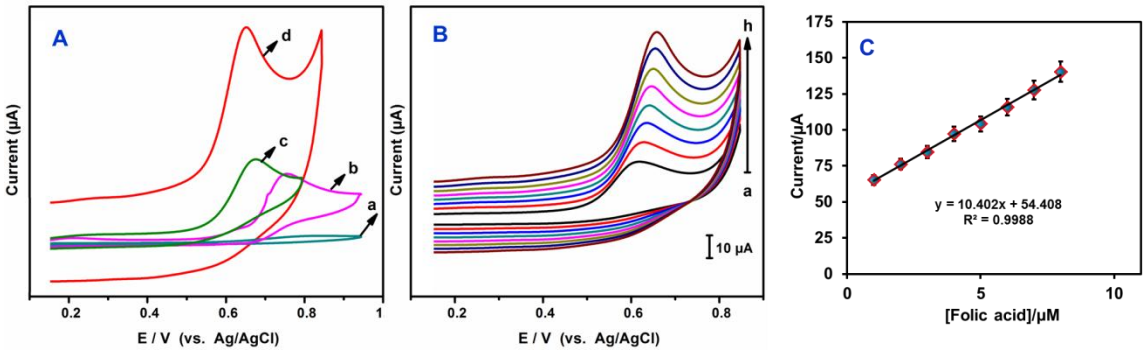

Figure 4. (A) Cyclic voltammograms obtained at unmodified SPCE (a) MoS_2/SPCE (b), GNS–MoS_2/SPCE (c) and GNS–MoS_2–AuNPs/SPCE (d) in phosphate buffer (pH 7.4) containing 2 μM FA. Scan rate = 50 mV s^{-1}. (B) Cyclic voltammograms obtained at GNS–MoS_2–AuNPs/SPCE towards different concentrations of FA (a to h; each 1 μM addition). (C) current/μM vs. [Folic acid]/μA.

3.2 Electrocatalysis of folic acid at GNS–MoS_2–AuNPs/SPCE

Figure 4A displays the cyclic voltammograms (CVs) obtained at unmodified SPCE (a) MoS_2/SPCE (b), GNS–MoS_2/SPCE (c) and GNS–MoS_2–AuNPs/SPCE in phosphate buffer containing 2 μM UA. The unmodified GCE shows poor electrocatalytic ability to oxidize FA. Comparatively, the MoS_2/SPCE and GNS–MoS_2/SPCE electrodes delivered sharp oxidation peaks for FA; however, the peak currents are lower and the oxidation potential is observed at high positive potential region which encounters high overpotential. Interestingly, GNS–MoS_2–AuNPs/SPCE has shown sharp oxidation peak with large peak currents at lower oxidation potential. The peak potential was + 0.62 V, while its onset potential was observed at + 0.50 V which is significantly lower than the previously reported

modified electrodes for FA oxidation [46-48]. Thus, GNS–MoS_2–AuNPs/SPCE nanocomposite provides better catalytic platform to FA, as a result the reaction is significantly accelerated which is evident from the great shift in overpotential. The strong synergic effect between the GNS, MoS_2 and AuNPs is greatly contributed to the higher electrocatalytic ability of the composite over individual components [27, 49]. The synergic combination of conductivity, surface area and catalytic ability of these materials can be highly beneficial for electrocatalytic applications.

Figure 4B displays the voltammograms obtained at GNS–MoS_2–AuNPs/SPCE in presence of different concentrations of FA. The catalytic current increases linearly as the concentration of FA increases which revealing efficient electrocatalysis without electrode fouling. The plot between oxidation peak current and concentration of FA exhibits good linearity (Figure 4C). Next, the influence of different scan rates (v) to the oxidation of FA at GNS–MoS_2–AuNPs/SPCE is investigated (Fig. 5A). The anodic peak current linearly as the scan rate increases. The plot between peak current and square root of scan rates exhibits good linearity indicating diffusion controlled process (Figure 5B) and this result is consistent with previously reported FA sensors [30, 34]

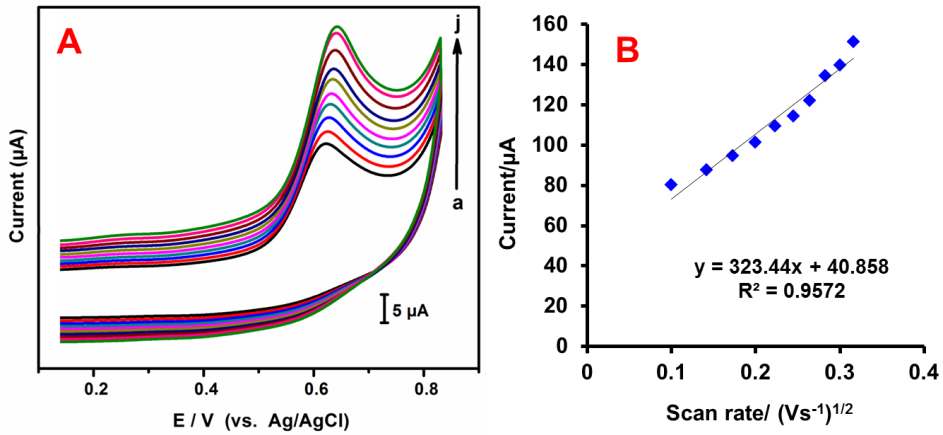

Figure 5. Effect of the scan rate: Cyclic voltammograms of GNS–MoS_2–AuNPs/SPCE towards 2 μM FA at different scan rates from 0.01 to 0.1 mV s^{-1}. (B) Plot of current vs. (scan rate)$^{1/2}$

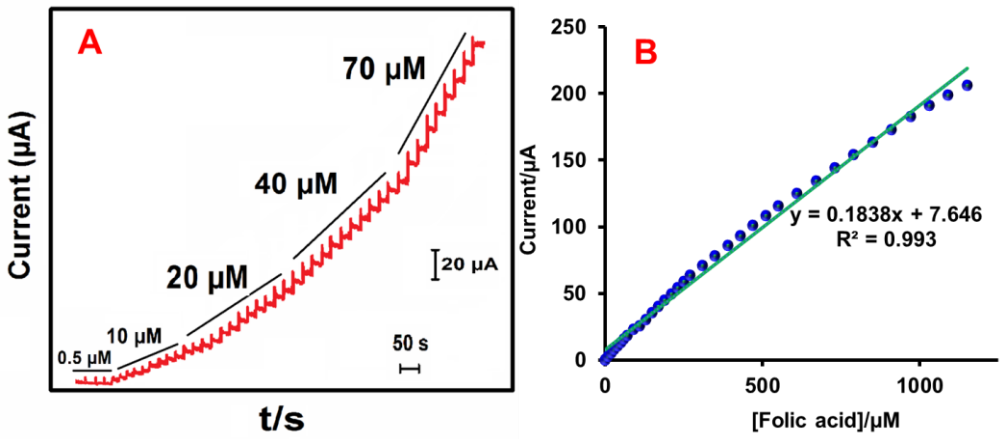

Figure 6. Amperometric response of GNS–MoS_2–AuNPs/SPCE upon each addition of 0.5 μM (a), 10 μM (b) 20 μM (c) and 40 μM (d) and 70 μM FA into continuously stirred phosphate buffer (pH 7.4). E_{app} = + 0.60 V

3.3 Amperometric determination FA

Fig. 6A displays the amperometric responses obtained at GNS–MoS_2–AuNPs/SPCE for sequential additions of FA. The applied potential was + 0.60 V. For each addition, a prompt and sensitive rise in the amperometric current is observed in the amperogram. Besides, the response current has reached 95% of steady-state current within 5s of FA injection indicating fast response time. The concentration dependent linear plot displayed good linearity (Fig. 5B). The working concentration range was linear from 50 nM–1150 μM with sensitivity of 0.8753 $\mu A \mu M^{-1}$ cm^{-2}. The limit of detection (LOD) was calculated as 38.5 nM. The LOD was calculated using the formula, LOD= 3 s_b/S where, s_b is the standard deviation of ten blank measurements and S is the sensitivity [50, 51]. The wide linear range, high sensitivity and low detection limit reveals the excellent sensor performance of the developed modified electrode. In addition, we have compared the sensor parameters such as LOD, sensitivity and linear range with previously reported modified electrodes (Table 1) [32, 35, 36, 45, 51–54]. As seen from the table, the GNS–MoS_2–AuNPs film has either superior or comparable sensor performance with previous reports. The excellent sensor performance is due to the synergic effect between GNS, MoS_2 and AuNPs. Moreover, we have adopted SPCE technology to prepare working electrode which has additional advantages since SPCE electrodes are cheaper and reproducible [52-54].

Table 1. Comparison of analytical parameters for the determination of FA at GNS–MoS_2–AuNPs film modified electrode with reported works

Electrode	Linear range/μM	LOD/nM	Ref.
methylene blue/Reduced graphene oxide	4–167	0.5	[33]
Pretreated boron-polycrystalline diamond	0.1–167	30	[36]
MoS_2/reduced graphene oxide	0.01–100	10	[37]
Porous silicon nanoparticles	1-1000	800	[46]
AuNPs modified gold electrode	0.01– 1	7.5	[55]
Fe_3O_4 nanoparticles	0.065–98	2	[56]
Ferrocenedicarboxylic acid/MWCNTs	4.6–152	1100	[57]
Hemoglobin/silica-coated magnetic nanoparticles	1–369	18	[58]
GNS–MoS_2–AuNPs/	0.05–1150	38.5	This work

3.4 Stability, repeatability and reproducibility

The stability of the fabricated electrode GNS–MoS_2–AuNPs/SPCE is tested by monitoring its sensing response to FA (0.1 μM) every day. During two weeks of continuous storage, the catalytic current slightly decreased in first two days and then attained a stable current. About 92.53% of the initial response current was retained after one month continuous use reveals good storage stability. The modified electrode exhibits appreciable repeatability with RSD of 3.52% for 5 repetitive measurements. Moreover, it exhibits good reproducibility with RSD of 3.16% for the five independent

measurements performed in five different modified SPCEs. Thus, the fabricated modified electrode displays good stability, repeatability and reproducibility and comparable to previous reports [30, 34].

3.5 Real sample analysis

Practical applicability of the GNS–MoS_2–AuNPs/SPCE for the determination of FA is verified in human urine sample. First human urine sample was collected from a healthy person and the sample was diluted with phosphate buffer (pH 7) in 1:50 ratio. 100 nM and 200 nM of FA are spiked and used to perform amperometry experiment. The added, found and recovery values are presented in Table 2. The recovery values are 97.16 to 98.55 % which is in satisfactory range to be used in real time applications [59]. Thus the developed sensor has great potential in practical applications.

Table 2. Determination of FA in spiked human urine sample using GNS–MoS_2–AuNPs/SPCE

Urine sample	Added/μM	Found/μM	Recovery/%	RSD*/%
FA	100	96.8	96.8	3.75
	200	196.1	98.0	4.50

* Relative Standard Deviation (RSD) of three individual measurements

4. CONCLUSIONS

In summary, a novel composite GNS–MoS_2–AuNPs was successfully prepared and the composite modified SPCE is more suitable for the determination of FA. The structure of the GNS–MoS_2–AuNPs was confirmed through SEM, EDX, EIS and electrochemical techniques**.** The synergic combination of GNS, MoS_2 and AuNPs greatly enhances the electrocatalysis and improved the overall sensor performance. The modified electrode has excellent sensor performance with wide linear range (50 nM–1150 μM), high sensitivity (0.8753 $\mu A \mu M^{-1} cm^{-2}$) and low detection limit (38.5 nM). The other advantages of the electrode are its reproducibility, sensitivity, selectivity, stability, repeatability, fast response time and low-cost fabrication. The advantages of SPCE technology in combination with excellent electrocatalytic attributes of GNS–MoS_2–AuNPs make this method highly suitable for FA sensor applications.

ACKNOWLEDGEMENT
This work was supported by the Ministry of Science and Technology (MOST), Taiwan (ROC).

References

1. V. Mani, S.-M. Chen, B.-S. Lou, *Int. J. Electrochem. Sci.,* 8 (2013) 11641.
2. Y. Shao, J. Wang, H. Wu, J. Liu, I.A. Aksay, Y. Lin, *Electroanalysis*, 22 (2010) 1027.
3. V. Mani, R. Devasenathipathy, S.-M. Chen, S.-T. Huang, V. Vasantha, *Enzyme Microb. Technol.,* 66 (2014) 60.
4. B. Devadas, V. Mani, S.-M. Chen, *Int. J. Electrochem. Sci.,* 7 (2012) 8064.

5. K. Kalantar-Zadeh, J.Z. Ou, *ACS Sensors*, 1 (2015) 5.
6. X. Gan, H. Zhao, X. Quan, *Biosens. Bioelectron.*, (2016). http://dx.doi.org/10.1016/j.bios.2016.03.042i.
7. Q.H. Wang, K. Kalantar-Zadeh, A. Kis, J.N. Coleman, M.S. Strano, *Nat. Nanotechnol.*, 7 (2012) 699.
8. W. Zheng, G. Li, L. Liu, W. Chen, W. Weng, W. Sun, *Int. J. Electrochem. Sci.*, 11 (2016) 7584
9. J.-W. Jiang, *Front. Phy.*, 10 (2015) 287.
10. B. Hinnemann, P.G. Moses, J. Bonde, K.P. Jørgensen, J.H. Nielsen, S. Horch, I. Chorkendorff, J.K. Nørskov, *J. Am. Chem. Soc.*, 127 (2005) 5308.
11. G. Sun, X. Zhang, R. Lin, J. Yang, H. Zhang, P. Chen, *Angew. Chem. Int. Ed.*, 127 (2015) 4734.
12. F. Zhou, S. Xin, H.W. Liang, L.T. Song, S.H. Yu, *Angew. Chem. Int. Ed.*, 53 (2014) 11552.
13. K. Chang, W. Chen, *ACS nano*, 5 (2011) 4720.
14. L. Xing, Z. Ma, *Microchim. Acta*, 183 (2016) 257.
15. V. Mani, M. Govindasamy, S.-M. Chen, R. Karthik, S.-T. Huang, *Microchim. Acta*, 183 (2016) 2267.
16. M. Govindasamy, V. Mani, S.-M. Chen, R. Karthik, K. Manibalan, R. Umamaheswari, *Int. J. Electrochem. Sci.*, 11 (2016) 2954.
17. A.K. Geim, I.V. Grigorieva, *Nature*, 499 (2013) 419.
18. N.A. Kumar, M.A. Dar, R. Gul, J.-B. Baek, *Mater. Today*, 18 (2015) 286.
19. H.Y. Kim, K.-N. Lee, M.-H. Lee, H.-U. Kim, C. Ahn, T. Kim, 2015 9th IEEE International Conference on, IEEE (2015) 80.
20. H. Long, A. Harley-Trochimczyk, T. Pham, Z. Tang, T. Shi, A. Zettl, C. Carraro, M.A. Worsley, R. Maboudian, *Adv. Funct. Mater.*, 26 (2016) 5158.
21. K.-J. Huang, L. Wang, J. Li, Y.-M. Liu, *Sens. Actuators, B*, 178 (2013) 671.
22. K. Pramoda, K. Moses, U. Maitra, C. Rao, *Electroanalysis*, 27 (2015) 1892.
23. P. Jing, H. Yi, S. Xue, Y. Chai, R. Yuan, W. Xu, *Anal. Chim. Acta*, 853 (2015) 234-241.
24. K. Zhao, W. Gu, L. Zhao, C. Zhang, W. Peng, Y. Xian, *Electrochim. Acta*, 169 (2015) 142-149.
25. H. Song, Y. Ni, S. Kokot, *Biosens. Bioelectron.*, 56 (2014) 137.
26. S. Su, W. Cao, C. Zhang, X. Han, H. Yu, D. Zhu, J. Chao, C. Fan, L. Wang, *RSC Adv.*, 6 (2016) 76614.
27. Q. Xiang, J. Yu, M. Jaroniec, *J. Am. Chem. Soc.*, 134 (2012) 6575.
28. Y. Shi, J.-K. Huang, L. Jin, Y.-T. Hsu, S.F. Yu, L.-J. Li, H.Y. Yang, *Sci. Rep.*, 3 (2013) 1839.
29. N. Lingappan, N.H. Van, S. Lee, D.J. Kang, *J. Power Sources*, 280 (2015) 39.
30. B. Unnikrishnan, Y.-L. Yang, S.-M. Chen, *Int. J. Electrochem. Sci.*, 6 (2011) 3224-3237.
31. B.B. Prasad, R. Madhuri, M.P. Tiwari, P.S. Sharma, *Sens. Actuators, B*, 146 (2010) 321.
32. M.M. Foroughi, H. Beitollahi, S. Tajik, A. Akbari, R. Hosseinzadeh, *Int. J. Electrochem.*, 9 (2014) 8407.
33. D. Zhang, X. Ouyang, W. Ma, L. Li, Y. Zhang, *Electroanalysis*, 28 (2016) 312.
34. P. Kalimuthu, S.A. John, *Biosens. Bioelectron.*, 24 (2009) 3575.
35. R.L. Gross, J. Reid, P.M. Newberne, B. Burgess, R. Marston, W. Hift, *Am. J. Clin. Nutr.*, 28 (1975) 225.
36. K. Cinková, Ľ. Švorc, P. Šatkovská, M. Vojs, P. Michniak, M. Marton, *Anal. Lett.*, 49 (2016) 107.
37. F. Chekin, F. Teodorescu, Y. Coffinier, G.-H. Pan, A. Barras, R. Boukherroub, S. Szunerits, *Biosens. Bioelectron.*, 85 (2016) 807.
38. M. Mazloum-Ardakani, M.A. Sheikh-Mohseni, M. Abdollahi-Alibeik, A. Benvidi, *Sens. Actuators, B*, 171 (2012) 380.
39. V. Mani, R. Devasenathipathy, S.-M. Chen, T.-Y. Wu, K. Kohilarani, *Ionics*, 21 (2015) 2675.
40. V. Mani, S.-T. Huang, R. Devasenathipathy, T.C. Yang, *RSC Adv.*, 6 (2016) 38463.
41. M. Govindasamy, S.-M. Chen, V. Mani, R. Devasenathipathy, R. Umamaheswari, K.J. Santhanaraj, A. Sathiyan, *J. colloid interf. Sci.*, 485 (2017) 129.

42. B. Dinesh, V. Mani, R. Saraswathi, S.-M. Chen, *RSC Adv.*, 4 (2014) 28229.
43. T.T. Shan, S. Xin, Y. You, H.P. Cong, S.H. Yu, A. Manthiram, *Angew. Chem. Int. Ed.*, 128 (2016) 12975.
44. S. Su, H. Sun, F. Xu, L. Yuwen, C. Fan, L. Wang, *Microchim. Acta*, 181 (2014) 1497.
45. A.J. Bard, L.R. Faulkner, Electrochemical methods: fundamentals and applications, Wiley New York, 1980.
46. T. Nie, L. Lu, L. Bai, J. Xu, K. Zhang, O. Zhang, Y. Wen, L. Wu, *Int. J. Electrochem. Sci.*, 8 (2013) 7016.
47. P. Kanchana, C. Sekar, *Spectrochim. Acta, Part A*, 137 (2015) 58.
48. T. Maiyalagan, J. Sundaramurthy, P.S. Kumar, P. Kannan, M. Opallo, S. Ramakrishna, *Analyst*, 138 (2013) 1779.
49. C. Rao, K. Gopalakrishnan, U. Maitra, *ACS Appl. Mater. Interfaces*, 7 (2015) 7809.
50. K. Manibalan, V. Mani, C.-H. Huang, S.-T. Huang, P.-C. Chang, *Analyst*, 140 (2015) 6040.
51. G.P. Keeley, A. O'Neill, M. Holzinger, S. Cosnier, J.N. Coleman, G.S. Duesberg, *Phys. Chem. Chem. Phys.*, 13 (2011) 7747.
52. J.-M. Zen, H.-P. Chen, A. Senthil Kumar, *Anal. Chim. Acta*, 449 (2001) 95.
53. N. Thiyagarajan, J.-L. Chang, K. Senthilkumar, J.-M. Zen, *Electrochem. Commun.*, 38 (2014) 86.
54. M. Thiruppathi, N. Thiyagarajan, M. Gopinathan, J.-M. Zen, *Electrochem. Commun.*, 69 (2016) 15.
55. L. Mirmoghtadaie, A.A. Ensafi, M. Kadivar, M. Shahedi, M.R. Ganjali, *Int. J. Electrochem. Sci.*, 8 (2013) 3755.
56. M.P. Kingsley, P.B. Desai, A.K. Srivastava, *J. Electroanal. Chem.*, 741 (2015) 71.
57. A.A. Ensafi, H. Karimi-Maleh, *J. Electroanal. Chem.*, 640 (2010) 75.
58. J. Ghodsi, A. Hajian, A.A. Rafati, Y. Shoja, O. Yurchenko, G. Urban, *J. Electrochem. Soc.*, 163 (2016) B609.
59. V. Mani, R. Devasenathipathy, S.-M. Chen, K. Kohilarani, R. Ramachandran, *Int. J. Electrochem. Sci*, 10 (2015) 1199.